

Numerical Shape Reconstruction for a Semi-Linear Elliptic Interface Inverse Problem

Yixin Tan¹ and Shengfeng Zhu^{2,*}

¹Department of Mathematics, East China Normal University, Shanghai 200241, China.

²Department of Mathematics & Key Laboratory of Mathematics and Engineering Applications (Ministry of Education) & Shanghai Key Laboratory of Pure Mathematics and Mathematical Practice, East China Normal University, Shanghai 200241, China.

Received 27 February 2023; Accepted (in revised version) 1 June 2023.

Abstract. We consider a shape reconstruction inverse problem constrained by a semi-linear elliptic interface problem in reaction diffusion. The existence of the model is shown. We perform shape sensitivity analysis and propose two numerical optimization algorithms based on the distributed shape gradient. The first algorithm allows shape changes and the second algorithm uses a level set method allowing shape and topological changes. Numerical results are presented to verify effectiveness of the algorithms.

AMS subject classifications: 49M41, 49N45

Key words: Shape reconstruction, distributed shape gradient, interface problem, semi-linear elliptic, level set method.

1. Introduction

Theoretical and numerical aspects of geometric inverse problems with unknown geometric shape have been investigated for many years. In various applications, an unknown subdomain and its complement are the sets where discontinuous parameters takes different constant values. Geometric inverse problems have wide applications in engineering, including heat source identification [14, 24], interface reconstruction of diffusive coefficient [16, 19, 21, 32], elastic inclusion detection [2], and electrical impedance tomography [10, 20].

For solving such problems, one needs to find a mechanism to represent the shape and follow its evolution. A straightforward method for solving such problems consists in parametrization of the shape, usually curve/surface and follow its evolution after regularization. However, this simple approach may fail if no topology information on recon-

*Corresponding author. *Email addresses:* 52265500020@stu.ecnu.edu.cn (Y. Tan), sfzhu@math.ecnu.edu.cn (S. Zhu)

struction is known a priori, especially for reconstruction of possible multi-connected components. Then, approaches and techniques allowing shape and topological changes are required, such as the level set method [1,8], phase-field method [5], and topological derivative approach [18,34]. A level set method was developed for numerically solving elliptic interface inverse problem [8,10,19] and inverse obstacle problem [30].

Shape optimization and reconstruction has caused interests not only on linear partial differential equation (PDE) constraints, but also on nonlinear PDE cases [12,18,31,34,40]. Interface location reconstruction was studied associated with linear elliptic problems [10,19] and linear elasticity [2,35]. For interface identification of semi-linear elliptic problems, sensitivity analysis was explored with the topological derivative [3] (see [5] for phase-field approach). Shape optimization of semi-linear elliptic problems is considered in [18,31,40]. In this paper, we consider an interface inverse problem associated with a semi-linear elliptic interface problem for chemical or heat reaction diffusion. We show existence of a solution to the optimization model and propose two numerical algorithms for reconstruction when the subdomain components are simply connected or multi-connected. Both the boundary moving and the level set method we propose rely on the objective's distributed shape gradient. The so-called shape gradient in the shape optimization community is contained in the Eulerian derivative, which measures the sensitivity information of the objective with respect to domain (shape) variations [33]. The Eulerian derivative is known to have two forms — viz. boundary type and volumetric one. The latter holds more generally, although they are equivalent when the boundary has certain smoothness [6,11]. Their discrete finite-element approximations behave different even when their formulations are equivalent on the continuous level. The boundary expression may work not well in certain optimization algorithms [38] (see [15,39] for possible theoretical explanations on the accuracy advantage of finite-element discretizations of distributed shape gradients). The distributed shape gradient has been applied in many problems including electrical impedance tomography [4,22], structural topology optimization [7], shape design of fluid flows [23], etc.

The rest of the paper is organized as follows. In Section 2, we introduce the interface inverse problem associated with a semi-linear elliptic boundary value problem. Then we show existence and perform shape sensitivity analysis. In Section 3, we propose two numerical algorithms based on shape gradient and level set method. In Section 4, numerical examples are presented to test performance of both algorithms. Brief conclusions follow in last section.

2. Existence and Shape Sensitivity of Model Problem

We first introduce an interface reconstruction inverse problem in nonlinear reaction diffusion, which can have applications in chemical diffusion processes or heat conduction. Then we show existence and perform shape sensitivity analysis with shape calculus. Let us first introduce notations for Sobolev spaces. Let $D \subset \mathbb{R}^d$, $d = 2, 3$ be an open bounded domain with Lipschitz boundary ∂D . The $L^\nu(D)$ function spaces are defined by

$$L^\nu(D) := \{u : \|u\|_{L^\nu(D)} < \infty\}, \quad \nu = 2, \infty,$$

where

$$\|f\|_{L^2(D)} := \left(\int_D |f(x)|^2 dx \right)^{1/2},$$

$$\|f\|_{L^\infty(D)} := \operatorname{ess\,sup} \{|f(x)| : x \in D\}.$$

Denote

$$H^1(D) = \{v \in L^2(D) : \nabla v \in L^2(D)^d\},$$

$$H_0^1(D) = \{v \in H^1(D) : v|_{\partial D} = 0\}$$

equipped with the norm

$$\|v\|_{H^1(D)} := \left(\|v\|_{L^2(D)}^2 + \|\nabla v\|_{L^2(D)}^2 \right)^{1/2}.$$

Let us make an assumption between the shape Ω and the fixed domain D . For the closed subsets $A, B \subset D$, denote

$$\varrho(A, B) = \max_{x \in A} \min_{y \in B} \|x - y\|,$$

where $\|\cdot\|$ is the Euclidean norm of a vector.

Assumption 2.1. There is a compact $K_0 \subset D$ such that $\Omega \subset\subset K_0$ and $\operatorname{dist}(\partial D, K_0) \geq d_0$ for some $d_0 > 0$, where $\operatorname{dist}(\partial D, K_0) = \sup(\varrho(\partial D, K_0), \varrho(K_0, \partial D))$.

2.1. Model problem and existence

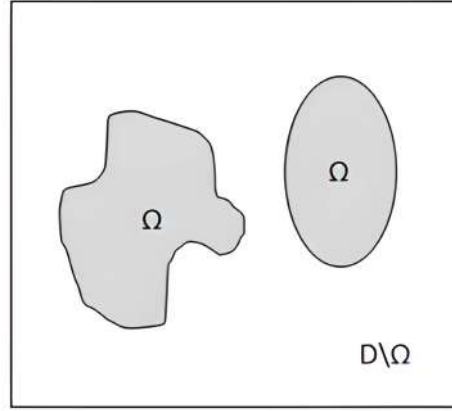
Let us introduce a measurable subset $\Omega \subset\subset D$, cf. Fig. 1. Consider the following semi-linear elliptic interface problem in chemical reaction diffusion or heat conductivity [27]:

$$\begin{aligned} -\nabla \cdot (k \nabla u) + u^3 &= f && \text{in } D, \\ \llbracket u \rrbracket &= 0 && \text{on } \partial \Omega, \\ \left[\left[k \frac{\partial u}{\partial n} \right] \right] &= 0 && \text{on } \partial \Omega, \\ u &= 0 && \text{on } \partial D, \end{aligned} \tag{2.1}$$

where n is the unit outward normal to the boundary $\partial \Omega$, $\llbracket \cdot \rrbracket$ the jump across the interface, $\Omega, D \setminus \bar{\Omega}$ are filled by materials with different respective positive diffusion coefficients or conductivities k_1, k_2 , and

$$k = \begin{cases} k_1 & \text{in } \Omega, \\ k_2 & \text{in } D \setminus \bar{\Omega}. \end{cases}$$

Here, k is called the diffusion coefficient in chemical diffusion processes or the thermal diffusivity in heat conduction problems and u denotes concentration or temperature.

Figure 1: Domains D and Ω .

The weak formulation of (2.1) is: Find $u \in H_0^1(D)$ such that

$$\int_D k \nabla u \cdot \nabla v dx + \int_D u^3 v dx = \int_D f v dx \quad \text{for all } v \in H_0^1(D). \quad (2.2)$$

It is known [9] that the problem (2.2) has a unique solution.

For $\Omega \subset\subset D$, define the perimeter of Ω in D as the total variation of its characteristic function χ_Ω , i.e.

$$P_D(\Omega) = \text{TV}(\chi_\Omega) := \sup \left\{ \int_\Omega \text{div} \phi dx \mid \phi \in \mathcal{D}^1(D, \mathbb{R}^d), \max_{x \in D} \|\phi(x)\| \leq 1 \right\},$$

where $\mathcal{D}^1(D, \mathbb{R}^d)$ denotes the space of all continuously differentiable functions with compact support in D . Consider a shape reconstruction inverse problem

$$\min_{\Omega \in \mathcal{U}_{\text{ad}}} J(\Omega) := \frac{1}{2} \int_M (u - u_d)^2 dx + \alpha P_D(\Omega), \quad (2.3)$$

where $u_d : H^1(\mathbb{R}^d) \rightarrow \mathbb{R}$ is a given smooth function, the admissible set \mathcal{U}_{ad} is a subset of $\mathcal{E}(D)$ with $\mathcal{E}(D)$ being the set of all subsets of D , the observation domain $M \subset D$, and $\alpha > 0$ is a regularization parameter. The second term is introduced for showing existence of a solution to the optimization model and for the regularization effect to the ill-posedness when observation contain possible noise in practice. If the boundary $\partial\Omega$ is Lipschitz continuous, then

$$P_D(\Omega) = \int_{\partial\Omega} ds.$$

This integral represents the curve length in 2D or the surface area in 3D. Here, the volumetric observation data are used to recover the interface between two different materials

in reaction diffusion. Though boundary observation seems to be more practical and complicated due to less data information available, we consider for simplicity distributed observation case typically on a partial banded region near the boundary rather than the whole domain. Actually, similar volumetric observation was considered for inverse obstacle problems associated with linear diffusion [8] and elliptic diffusive interface reconstruction [19]. Interface reconstruction of semi-linear elliptic problems has other applications — e.g. in cardiac electrophysiology [3, 5], where homogeneous Neumann boundary conditions are satisfied and boundary observation is employed.

To obtain theoretical existence of the model problem, we consider the set of characteristic functions

$$\text{Char}(D) = \{\chi \in L^2(D) \mid \chi(1 - \chi) = 0 \text{ a.e. in } D\}$$

equipped with the $L^2(D)$ topology, where

$$\chi = \chi_\Omega = \begin{cases} 1 & \text{in } \Omega, \\ 0 & \text{in } D \setminus \bar{\Omega}. \end{cases}$$

Theorem 2.1. *The mapping $\chi_\Omega \mapsto u(\Omega)$ with $u(\Omega)$ denoting the weak solution to problem (2.2) is continuous from $\text{Char}(D)$ into $H_0^1(D)$.*

Proof. Let $\Omega_i, i = 1, 2, \dots$, and Ω_0 be a measurable subset of $D \subset \mathbb{R}^d$, $u_i = u(\Omega_i)$, $i = 1, 2, \dots$ the solution to (2.2) with the domain Ω_i , and

$$\begin{aligned} k &= k_1 \chi_{\Omega_0} + k_2 (1 - \chi_{\Omega_0}), \\ \tilde{k} &= k_1 \chi_{\Omega_i} + k_2 (1 - \chi_{\Omega_i}). \end{aligned}$$

Then

$$k - \tilde{k} = (k_1 - k_2)(\chi_{\Omega_0} - \chi_{\Omega_i}).$$

For k and \tilde{k} , there exists respective unique solutions $u_0 \in H_0^1(D)$ and $u_i \in H_0^1(D)$ such that

$$\begin{aligned} \int_D k \nabla u_0 \cdot \nabla v + u_0^3 v dx &= \int_D f v dx \quad \text{for all } v \in H_0^1(D), \\ \int_D \tilde{k} \nabla u_i \cdot \nabla v + u_i^3 v dx &= \int_D f v dx \quad \text{for all } v \in H_0^1(D). \end{aligned} \tag{2.4}$$

By (2.4), we have

$$\begin{aligned} &\int_D \tilde{k} (\nabla u_0 - \nabla u_i) \cdot \nabla v + (u_0^3 - u_i^3) v dx \\ &= - \int_D (k - \tilde{k}) \nabla u_0 \cdot \nabla v dx \quad \text{for all } v \in H_0^1(D). \end{aligned}$$

Taking $v = u_0 - u_i$, we obtain

$$\begin{aligned} & \int_D \tilde{k} |\nabla u_0 - \nabla u_i|^2 dx + \int_D \int_0^1 3(su_i + (1-s)u_0)^2 (u_0 - u_i)^2 ds dx \\ &= - \int_D (k - \tilde{k}) \nabla u_0 \cdot (\nabla u_0 - \nabla u_i) dx, \end{aligned}$$

which implies that

$$\begin{aligned} & \min\{k_1, k_2\} \|\nabla u_0 - \nabla u_i\|_{L^2(D)}^2 \\ & \leq \int_D |(k_1 - k_2)(\chi_{\Omega_0} - \chi_{\Omega_i})| \cdot |\nabla u_0 \cdot (\nabla u_0 - \nabla u_i)| dx \\ & \leq \|(k_1 - k_2)(\chi_{\Omega_0} - \chi_{\Omega_i}) \cdot \nabla u_0\|_{L^2(D)} \|\nabla u_0 - \nabla u_i\|_{L^2(D)}. \end{aligned}$$

Then, we have

$$\min\{k_1, k_2\} \|\nabla u_0 - \nabla u_i\|_{L^2(D)} \leq \|(k_1 - k_2)(\chi_{\Omega_0} - \chi_{\Omega_i}) \cdot \nabla u_0\|_{L^2(D)}. \quad (2.5)$$

The family of domains $\Omega_i, i = 1, 2, \dots$, is said to converge in measure to the domain Ω_0 if the sequence of characteristic functions χ_{Ω_i} converges to χ_{Ω_0} in the set $\text{Char}(D)$, i.e. in $L^2(D)$ norm. Then the sequence of functions $g_i := (k_1 - k_2)(\chi_{\Omega_0} - \chi_{\Omega_i})$ converges to zero in $L^2(D)$ as $i \rightarrow \infty$. Therefore, we have $\|g_i(x)\| \leq \text{const}$. By the Lebesgue dominated convergence theorem, there exists a subsequence $\{g_{i_j}\}_{j=1}^\infty$ such that $g_{i_j}(x) \rightarrow 0$ as $j \rightarrow \infty$ for almost every x in \bar{D} . Then the function g_i on the right-hand side of (2.5) belongs to $L^1(D)$, and converges to zero for almost every x in \bar{D} . Then the right-hand side of (2.5) converges to zero as $i \rightarrow \infty$. Thanks to (2.5), one can show that the norm $\|\nabla(u_i - u_0)\|_{L^2(D)}$ converges to zero, and by the Poincaré inequality of $H_0^1(D)$ we have that $\|u_i - u_0\|_{H^1(D)} \rightarrow 0$, hence the desired continuity. \square

Theorem 2.2. *The shape functional (2.3) is lower semi-continuous on the set $\text{Char}(D) \subset L^2(D)$.*

Proof. For the second term of (2.3), the functional $\chi_\Omega \mapsto P_D(\Omega)$ is semi-continuous on the set $\text{Char}(D)$ [33, Lemma 2.6]. Let $u \in H_0^1(D)$ (resp. $\tilde{u} \in H_0^1(D)$) be the unique solution of (2.4) associated with Ω (resp. $\tilde{\Omega}$). For the first term of (2.3), the Lipschitz continuity can be obtained as follows:

$$\begin{aligned} & \frac{1}{2} \int_M (u - u_d)^2 - \frac{1}{2} \int_M (\tilde{u} - u_d)^2 \\ &= \frac{1}{2} \int_D \chi_M (u - \tilde{u})(u - \tilde{u} + 2\tilde{u} - 2u_d) \\ & \leq \frac{1}{2} \|\chi_M\|_{L^\infty(D)} \|u - \tilde{u}\|_{L^2(D)} \|u - \tilde{u} + 2\tilde{u} - u_d\|_{L^2(D)} \\ & \leq \frac{1}{2} \|u - \tilde{u}\|_{L^2(D)} (\|u - \tilde{u}\|_{L^2(D)} + 2\|\tilde{u} - u_d\|_{L^2(D)}). \end{aligned}$$

Now we can conclude that $J(\Omega)$ is lower semi-continuous on $\text{Char}(D)$ by Theorem 2.1. \square

For any constant $C > 0$,

$$\text{Char}(D, C) = \{\chi_\Omega \in \text{Char}(D) \mid P_D(\Omega) \leq C\}.$$

Setting $\mathcal{J}(\chi) = J(\Omega)$, $u = u(\chi)$, we write the problem (2.3) as

$$\min_{\chi \in \text{Char}(D, C)} \mathcal{J}(\chi) = \frac{1}{2} \int_M (u(\chi) - u_d)^2 dx + \alpha \text{TV}(\chi). \quad (2.6)$$

Theorem 2.3. *Problem (2.6) admits at least one solution.*

Proof. It obviously holds that $\mathcal{J}(\chi) \geq 0$ from the form of $\mathcal{J}(\chi)$. Thus, the value

$$\inf_{\chi \in \text{Char}(D, C)} \mathcal{J}(\chi)$$

exists. For a sequence of subdomains $\{\Omega_n\}_{n=0}^\infty$, denote $\chi_n = \chi_{\Omega_n}$. Let $\{\chi_n\}_{n=0}^\infty \subset \text{Char}(D)$ be a minimization sequence — i.e.

$$\lim_{n \rightarrow \infty} \mathcal{J}(\chi_n) = \inf_{\chi \in \text{Char}(D, C)} \mathcal{J}(\chi). \quad (2.7)$$

By [33, Proposition 2.8], the set $\text{Char}(D, C)$ is compact in $L^2(D)$. Therefore, there exists a subsequence (still denoted by $\{\chi_n\}_{n=0}^\infty$) and a measurable set $\Omega^* \subset D$ such that $\chi_n \rightarrow \chi^*$ tends to $n \rightarrow \infty$ with $\chi^* = \chi_{\Omega^*}$. By Theorem 2.2, we have

$$\lim_{n \rightarrow \infty} \inf \mathcal{J}(\chi_n) \geq \mathcal{J}(\chi^*).$$

Then by (2.7),

$$\lim_{n \rightarrow \infty} \mathcal{J}(\chi_n) = \inf_{\chi \in \text{Char}(D, C)} \mathcal{J}(\chi) \geq \mathcal{J}(\chi^*).$$

Since

$$\inf_{\chi \in \text{Char}(D, C)} \mathcal{J}(\chi) \leq \mathcal{J}(\chi^*),$$

we obtain that χ^* is a minimizer — i.e.

$$\mathcal{J}(\chi^*) = \min_{\chi \in \text{Char}(D, C)} \mathcal{J}(\chi).$$

The proof is complete. \square

Before analysing the shape sensitivity, we use the Lagrange multiplier method to deal with the constraint of the semi-linear elliptic problem. We first introduce the Lagrangian

$$L(\Omega, v, q) := \int_D \frac{1}{2} \chi_M (v - u_d)^2 dx - \int_D k \nabla v \cdot \nabla q dx - \int_D v^3 q dx + \int_D f q dx + \alpha P_D(\Omega),$$

where the functions v, q are in $H_0^1(D)$. The saddle-point of $L(\Omega, v, q)$ is characterized by the first-order optimality condition

$$\left\langle \frac{\partial L(\Omega, v, q)}{\partial v}, \phi \right\rangle_D = \left\langle \frac{\partial L(\Omega, v, q)}{\partial q}, \phi \right\rangle_D = 0$$

for all $\phi \in H_0^1(D)$. By the density, this leads to the adjoint problem

$$\begin{aligned}
-\nabla \cdot (k\nabla p) + 3u^2 p &= \chi_M(u - u_d) && \text{in } D, \\
[[p]] &= 0 && \text{on } \partial\Omega, \\
\left[\left[k \frac{\partial p}{\partial n} \right] \right] &= 0 && \text{on } \partial\Omega, \\
p &= 0 && \text{on } \partial D,
\end{aligned} \tag{2.8}$$

and the state problem (2.1).

2.2. Shape sensitivity analysis

Shape sensitivity analysis is a valuable tool to design numerical methods for shape optimization [33]. We analyse the shape sensitivity for our shape reconstruction problem with the perturbation of identity method [13], which is equivalent to the velocity method [33] in the sense of first-order Taylor expansion. For $t \in [0, \varepsilon]$, $\varepsilon > 0$, define a family of smooth mappings $\{F_t\}_{t \in [0, \varepsilon]}$ with $F_t : \bar{D} \rightarrow \bar{D}$ mapping the initial (reference) sub-domain to a perturbed sub-domain. The boundary ∂D is fixed — i.e. $F_t(\partial D) = \partial D$. Then we denote $\Omega_t := F_t(\Omega) = \{F_t(x) : x \in \Omega\}$ with $\Omega_0 = \Omega$ and the boundary $\partial\Omega_t := F_t(\partial\Omega) = \{F_t(x) : x \in \partial\Omega\}$ with $\partial\Omega_0 = \partial\Omega$. The mappings $\{F_t\}_{t \in [0, \varepsilon]}$ describe the motion of each point in D , i.e. at $t \in [0, \varepsilon]$, the point $x \in D$ has a new position $x_t := F_t(x) \in D$ with $x_0 = x$. More precisely,

$$F_t = \text{Id} + tV,$$

where Id the identity mapping and $V = V(x)$ denotes a sufficiently smooth vector field in

$$V_{\text{ad}} = \{V \in W^{1, \infty}(D, \mathbb{R}^d) : V = 0 \text{ on } \partial D\}.$$

Here, $W^{1, \infty}(D, \mathbb{R}^d)$ is the space of vector field functions for which each of its components belongs to $W^{1, \infty}(D)$, a Banach space of functions uniformly bounded up to first-order weak derivative.

Definition 2.1. Let $V \in V_{\text{ad}}$ and $\varphi \in H^1(D)$. Define on the boundary $\partial\Omega$ the tangential part of V

$$V_\Gamma := V - (V \cdot n)n,$$

and the tangential divergence of V

$$\text{div}_\Gamma V := \text{div} V - n^T \nabla V n,$$

where $\nabla V := (\partial V_i / \partial x_j)_{1 \leq i, j \leq d}$. Define the tangential gradient of φ

$$\nabla_\Gamma \varphi = \nabla \varphi - \frac{\partial \varphi}{\partial n} n.$$

Definition 2.2. For a real-valued shape functional $J : \Omega \mapsto \mathbb{R}$, the Eulerian derivative of J at Ω in a direction $V \in V_{\text{ad}}$ is defined by the following limit:

$$dJ(\Omega; V) := \lim_{t \searrow 0} \frac{J(\Omega_t) - J(\Omega)}{t}.$$

The shape functional depends both on Ω and a field variable, which describes a PDE defined on a domain related to Ω . Then, shape sensitivity analysis of the field variable — e.g. $u = u(\Omega)$ is naturally necessary. Let u and u_t be two state quantities related to domains Ω and Ω_t , respectively. The set $Q \subset \mathbb{R}^{d+1}$, where $Q = \cup_{t \in [0, t_0]} \{t\} \times \Omega_t$, determines the evolution of Ω in space and time $t \in [0, t_0]$. The function u_t can be viewed as the restriction of another function $\{t\} \times \Omega_t$ to $u : Q \rightarrow \mathbb{R}$, $u(t, x + tV(x)) = u_t(x_t)$ for $x \in \Omega$ and $t \in [0, \varepsilon]$. Suppose that u is smooth enough in a δ -neighborhood Ω_δ of Ω . Then,

Definition 2.3. Material and shape derivatives of u at $x \in D$ can be defined if there exist limits

$$\dot{u}(x) = \lim_{t \searrow 0} \frac{u(t, x + tV(x)) - u(0, x)}{t} = \left. \frac{d}{dt} u(t, x + tV(x)) \right|_{t=0}$$

and

$$u'(x) = \lim_{t \searrow 0} \frac{u(t, x) - u(0, x)}{t},$$

respectively.

It is easy to verify that

$$\dot{u}(x) = u'(x) + \nabla u(x) \cdot V(x).$$

By definition and simple calculation, for any $\varphi, \vartheta \in H^1(D)$ the following relationships hold:

$$(\varphi \vartheta)^\cdot = \dot{\varphi} \vartheta + \varphi \dot{\vartheta}, \quad (\nabla \varphi)^\cdot = \nabla \dot{\varphi} - \nabla V^\top \nabla \varphi, \quad (\nabla \varphi)^\cdot = \nabla \dot{\varphi} - \nabla \varphi \nabla V. \quad (2.9)$$

Let Q_δ be a δ -neighborhood of Q and $g : Q_\delta \rightarrow \mathbb{R}$ a sufficiently smooth function. Consider the shape functionals

$$J_1(t; \Omega) = \int_{\Omega} g(t, x_t) dx,$$

$$J_2(t; \Omega) = \int_{\partial \Omega} g(t, x_t) ds.$$

Lemma 2.1 (cf. Haslinger & Mäkinen [13, Lemma 3.3]).

$$\left. \frac{dJ_1(\cdot; \Omega)}{dt} \right|_{t=0} = \int_{\Omega} \dot{g} + g \operatorname{div} V dx,$$

$$\left. \frac{dJ_2(\cdot; \Omega)}{dt} \right|_{t=0} = \int_{\partial \Omega} \dot{g} + g \operatorname{div}_\Gamma V ds.$$

The following theorem introduces shape sensitivity analysis results of the shape reconstruction problem. The shape gradient of the shape functional can be expressed in a volumetric integral and a boundary integral if the boundary is sufficiently smooth.

Theorem 2.4. *Let u be the weak solution of (2.2). Assume that $\Omega \subset D$ is Lipschitz. Then, $J(\Omega)$ is shape differentiable at any $\Omega \in \mathcal{U}_{ad}$, and the Eulerian derivative reads in a volume form (except for the last term)*

$$\begin{aligned} dJ(\Omega; V) = & \int_D k \nabla u^T (\nabla V + \nabla V^T) \nabla p + \nabla f \cdot V p \\ & + \operatorname{div} V \left(\frac{1}{2} (u - u_d)^2 - k \nabla u \cdot \nabla p - u^3 p + f p \right) dx + \alpha \int_{\partial \Omega} \operatorname{div}_\Gamma V ds. \end{aligned} \quad (2.10)$$

If the boundary $\partial \Omega$ is C^2 , the boundary formulation of the Eulerian derivative holds

$$dJ(\Omega; V) = \int_{\partial \Omega} \left\{ \frac{(k_1 - k_2)}{k_1 k_2} \left[k_1 k_2 \nabla_\Gamma u \cdot \nabla_\Gamma p + \left(k \frac{\partial u}{\partial n} \right) \left(k \frac{\partial p}{\partial n} \right) \right] + \alpha \kappa \right\} V \cdot n ds, \quad (2.11)$$

where $\kappa = \operatorname{div} n$ denotes the mean curvature.

Proof. We give a formal yet not strict derivation. Notice that the shape functional can be written in the form of the Lagrangian

$$J(\Omega) = L(\Omega, u, p) = \int_D j(u) \chi_M dx - \int_D k \nabla u \cdot \nabla p dx - \int_D u^3 p dx + \int_D f p dx + \alpha P_D(\Omega),$$

where $j(u) = 1/2(u - u_d)^2$. Using Lemma 2.1 and taking partial derivative with respect to t , we have

$$\begin{aligned} dJ(\Omega; V) = & \int_D (j(u) \chi_M + f p - (k \nabla u) \cdot \nabla p - u^3 p) \\ & + \operatorname{div} V (j(u) \chi_M + f p - k \nabla u \cdot \nabla p - u^3 p) dx + \alpha \int_{\partial \Omega} \operatorname{div}_\Gamma V ds. \end{aligned}$$

It follows from (2.9) that

$$\begin{aligned} dJ(\Omega; V) = & \int_D (u - u_d) \dot{u} \chi_M + \dot{f} p + f \dot{p} - k \nabla \dot{u} \cdot \nabla p - k \nabla u \cdot \nabla \dot{p} \\ & + k \nabla u^T (\nabla V + \nabla V^T) \nabla p - 3u^2 \dot{u} p - u^3 \dot{p} \\ & + \operatorname{div} V (j(u) \chi_M + f p - k \nabla u \cdot \nabla p - u^3 p) dx + \alpha \int_{\partial \Omega} \operatorname{div}_\Gamma V ds. \end{aligned}$$

Integrating by parts and sorting, we obtain

$$dJ(\Omega; V) = \int_D ((u - u_d) \chi_M + \nabla \cdot (k \nabla p) - 3u^2 p) \dot{u} + (f + \nabla \cdot (k \nabla u) - u^3) \dot{p}$$

$$\begin{aligned}
& + \nabla f \cdot V p + k \nabla u^T (\nabla V + \nabla V^T) \nabla p \\
& + \operatorname{div} V (j(u) \chi_M + f p - k \nabla u \cdot \nabla p - u^3 p) dx + \alpha \int_{\partial \Omega} \operatorname{div}_\Gamma V ds. \quad (2.12)
\end{aligned}$$

According to the Eqs. (2.1) and (2.8), we can rewrite (2.12) as (2.10).

To show the boundary formulation (2.11), integration by parts for (2.10) implies that

$$\begin{aligned}
dJ(\Omega; V) &= \int_D V \cdot (-f \nabla p - (u - u_d) \chi_M \nabla u + 3u^2 p \nabla u + u^3 \nabla p) dx \\
&+ \int_D ((\nabla V + \nabla V^T) - (\operatorname{div} V) I) k \nabla u \cdot \nabla p dx + \alpha \int_{\partial \Omega} \kappa V \cdot n ds, \quad (2.13)
\end{aligned}$$

where I denotes the identity matrix. Let us denote two phases $\Omega_1 := \Omega$ and $\Omega_2 := D \setminus \overline{\Omega}$ and $u_i \in H^1(\Omega_i)$ be the restriction of u to Ω_i , $i = 1, 2$. Then

$$\begin{aligned}
u_1 &= u_2 && \text{in } H^{1/2}(\partial \Omega), \\
k_1 \frac{\partial u_1}{\partial n} &= k_2 \frac{\partial u_2}{\partial n} && \text{in } H^{-1/2}(\partial \Omega),
\end{aligned}$$

where $H^{1/2}(\partial \Omega)$ denotes the trace space of functions in $H_0^1(D)$ and $H^{-1/2}(\partial \Omega)$ denotes the dual of $H^{1/2}(\partial \Omega)$. Therefore, we can decompose the integrals in (2.13) on Ω_1 and Ω_2

$$\begin{aligned}
dJ(\Omega; V) &= \sum_{i=1}^2 \left(\int_{\Omega_i} V \cdot (-f \nabla p_i - (u_i - u_d) \chi_M \nabla u_i + 3u_i^2 p_i \nabla u_i + u_i^3 \nabla p_i) dx \right. \\
&\quad \left. + \int_{\Omega_i} ((\nabla V + \nabla V^T) - (\operatorname{div} V) I) k \nabla u_i \cdot \nabla p_i dx \right) + \alpha \int_{\partial \Omega} \kappa V \cdot n ds. \quad (2.14)
\end{aligned}$$

Using integration by parts and taking into account that

$$\begin{aligned}
-\nabla \cdot (k \nabla u) + u^3 &= f, \\
-\nabla \cdot (k \nabla p) + 3u^2 p &= (u - u_d) \chi_M
\end{aligned}$$

in D , we write

$$\begin{aligned}
& \int_{\Omega_i} V \cdot (-f \nabla p_i - (u_i - u_d) \chi_M \nabla u_i + 3u_i^2 p_i \nabla u_i + u_i^3 \nabla p_i) dx \\
& + k_i \int_{\Omega_i} ((\nabla V + \nabla V^T) - (\operatorname{div} V) I) \nabla u_i \cdot \nabla p_i dx \\
& = \operatorname{Sign} \int_{\partial \Omega} k_i \left((\nabla u_i \cdot \nabla p_i) V \cdot n - (\nabla u_i \cdot V) \frac{\partial p_i}{\partial n} - (\nabla p_i \cdot V) \frac{\partial u_i}{\partial n} \right) ds, \quad i = 1, 2, \quad (2.15)
\end{aligned}$$

where

$$\operatorname{Sign} = \begin{cases} 1, & \text{if } i = 1, \\ -1, & \text{if } i = 2. \end{cases}$$

This difference is a consequence of the fact that n is pointing outward Ω_1 . We can introduce the continuous quantities across the boundary. Then, the straightforward calculation yields

$$\begin{aligned}
& \int_{\Omega_i} V (-f \nabla p_i - (u_i - u_d) \chi_M \nabla u_i + 3u_i^2 \nabla u_i p_i + u_i^3 \nabla p_i) dx \\
& + k_i \int_{\Omega_i} ((\nabla V + \nabla V^T) - (\operatorname{div} V) I) \nabla u_i \cdot \nabla p_i dx \\
= & \operatorname{Sign} \left(\int_{\partial\Omega} \left(k_i \nabla_{\Gamma} u_i \cdot \nabla_{\Gamma} p_i - \frac{1}{k_i} \left(k_i \frac{\partial u_i}{\partial n} \right) \left(k_i \frac{\partial p_i}{\partial n} \right) \right) V \cdot n \right. \\
& \left. - \int_{\partial\Omega} \left((\nabla_{\Gamma} u_i \cdot V_{\Gamma}) \left(k_i \frac{\partial p_i}{\partial n} \right) + (\nabla_{\Gamma} p_i \cdot V_{\Gamma}) \left(k_i \frac{\partial u_i}{\partial n} \right) \right) \right), \quad i = 1, 2. \quad (2.16)
\end{aligned}$$

Combining (2.14) and (2.16), we finally get the desired surface expression (2.11). \square

3. Numerical Optimization Algorithms

In this section, we present two optimization algorithms for solving the model problem. Both algorithms are built on the distributed shape gradients derived in last section and can have shape changes in optimization. They differ in that the first algorithm moves meshes during optimization, while the second algorithm based on the level set method can have topological changes on fixed meshes. The distributed shape gradient formulation was recently adopted in solving inverse problems [12, 22] and was expected to be more robust than the popular boundary formulation of shape gradient.

At each iteration of the outer optimization loop, we use the Galerkin finite element method in order to discretize:

- (i) State equation.
- (ii) Adjoint problem.
- (iii) Shape gradient flow.
- (iv) Level set transport equation.
- (v) Reinitialization.

The continuous piecewise linear polynomials are used. In this paper, we do not address the situation of high contrast ratio between the two phases in the diffusion coefficient. In that case, reliable approaches such as immersed interface method [19] or cut finite element method [7] could be used. We consider simple (usual) finite element discretizations of the state and adjoint interface problems. We use Newton's method to solve the nonlinear state problem (2.2).

3.1. Algorithm 1

During shape changes associated with mesh moving, the mesh quality may decrease, especially for large domain deformations. Remeshing is performed frequently in shape optimization to produce quasi-uniform meshes desirable for finite element discretizations [38]. We use the conformal transformation [17] rather than remeshing to retain the mesh quality in 2D. We remark that in [17] the mesh quality preserving strategy is used in deformations on the variable domain Ω , while here the conformal transformation is employed for interface evolution on the fixed design region D . Let us introduce the idea.

The classical H -shape gradient of J at Ω with respect to $(H, (\cdot, \cdot)_H)$ is defined as the unique element $\nabla J(\Omega) \in H$ that satisfies

$$(\nabla J(\Omega), V)_H = -dJ(\Omega; V) \quad \text{for all } V \in H.$$

Notice that the H -shaped gradient itself is the minimizer of the problem

$$\min_{V \in H} \frac{1}{2} \|V\|_H^2 + dJ(\Omega; V).$$

To retain mesh quality, the H -shape gradient can be modified by a conformal transformation. A vector field $V = (V_1, V_2) \in [C^1(\bar{D})]^2$ is called holomorphic if it satisfies the Cauchy-Riemann equations on D , i.e.

$$\begin{aligned} \partial_{x_1} V_1 &= \partial_{x_2} V_2, \\ \partial_{x_2} V_1 &= -\partial_{x_1} V_2. \end{aligned}$$

These conditions can be written as $\mathcal{B}V = 0$, where the operator \mathcal{B} is defined as

$$\mathcal{B} := \begin{pmatrix} -\partial_{x_1} & \partial_{x_2} \\ \partial_{x_2} & \partial_{x_1} \end{pmatrix}, \quad [C^1(\bar{D})]^2 \rightarrow [C^0(\bar{D})]^2.$$

A holomorphic mapping is called conformal if it is injective.

An H -shape gradient satisfying the Cauchy-Riemann can be obtained by solving the constrained optimization problem

$$\min_{\substack{V \in H, \\ \mathcal{B}V=0}} \frac{1}{2} \|V\|_H^2 + dJ(\Omega; V). \quad (3.1)$$

A regularized version with the penalization of (3.1) reads

$$\min_{V \in H} \frac{1}{2} \left(\frac{1}{\gamma} \|\mathcal{B}V\|_{L^2(D)}^2 + \|V\|_H^2 \right) + dJ(\Omega; V),$$

where $\gamma > 0$ is a penalty factor. For our model problem, choose a space of deformations that is frequently used, which is the space $H = [\hat{H}^1(D)]^2$ consisting of all functions $V \in [H^1(\Omega)]^2$ with mean zero. This space becomes a Hilbert space when equipped with the inner product

$$(U, V)_{\hat{H}^1} := (\nabla U, \nabla V)_{[L^2]^{2 \times 2}}.$$

Define the symmetric and antisymmetric parts of the derivative ∇U by

$$S(\nabla U) := \frac{1}{2}(\nabla U + \nabla U^\top), \quad AS(\nabla U) := \frac{1}{2}(\nabla U - \nabla U^\top).$$

Therefore, for any $U \in [H^1(\Omega)]^2$ it holds that

$$\|\nabla U\|_{[L^2]^{2 \times 2}}^2 = \|S(\nabla U)\|_{[L^2]^{2 \times 2}}^2 + \|AS(\nabla U)\|_{[L^2]^{2 \times 2}}^2.$$

Observe that

$$\|AS(\nabla U)\|_{[L^2]^{2 \times 2}}^2 = \|\partial_{x_1} U_2 - \partial_{x_2} U_1\|_{L^2}^2,$$

and hence attempting to minimize this term, could be counterproductive when also trying to closely satisfy the Cauchy-Riemann equations, as they require $\partial_{x_1} U_2 + \partial_{x_2} U_1 = 0$.

Therefore, we define directly

$$\mathcal{Q} := \left\{ V \in [L^2(D)]^2 : S(\nabla V) \in [L^2(D)]^{2 \times 2}, V = 0 \text{ on } \partial D, \text{ and } \int_{\Omega} \partial_{x_2} V_1 + \partial_{x_1} V_2 = 0 \right\}.$$

We equip \mathcal{Q} with the inner product

$$(U, V)_{\mathcal{Q}} = \frac{1}{\gamma} (\mathcal{B}U, \mathcal{B}V)_{[L^2(D)]^2} + (S(\nabla U), S(\nabla V))_{[L^2(D)]^{2 \times 2}}.$$

Consider

$$\min_{V \in \mathcal{Q}} \frac{1}{2} \left(\frac{1}{\gamma} \|\mathcal{B}V\|_{L^2(D)}^2 + \|S(\nabla V)\|_{[L^2(D)]^{2 \times 2}}^2 \right) + dJ(\Omega; V),$$

whose equivalent (descent) shape gradient flow with a nearly conforming mapping — i.e. the variational form is: Find a $U \in \mathcal{Q}$ such that

$$(U, V)_{\mathcal{Q}} = -dJ(\Omega; V) \quad \text{for all } V \in \mathcal{Q}.$$

Algorithm 1: Shape Reconstruction of Diffusive Interface

- 1 Initialization.
 - 2 **while** Objective functional changes as iteration **do**
 - 3 Solve the state problem with Newton's method.
 - 4 Solve the adjoint state.
 - 5 Solve the shape gradient flow with nearly conformal mapping.
 - 6 Deformation evolution $\Omega^{m+1} \leftarrow \Omega^m + \eta U^m$.
 - 7 **end**
-

In our numerical experiment, we choose the fixed value $\eta = 0.01$ as the step size of the grid movement. It is worth noting that Algorithm 1 is only suited for the case $d = 2$.

3.2. Algorithm 2

The second algorithm that we propose is based on the level set method [25,26]. We first introduce the basics of the level set method to represent subdomains and track interfaces. Consider domains D and Ω described above. The domain D is divided into two subregions Ω and $D \setminus \Omega$ by $\partial\Omega$. A level set function $\phi : D \rightarrow \mathbb{R}$ is introduced to satisfy

$$\begin{aligned}\phi(x) &< 0, & x \in \Omega, \\ \phi(x) &= 0, & x \in \partial\Omega, \\ \phi(x) &> 0, & x \in D \setminus \overline{\Omega}.\end{aligned}$$

The Heaviside and delta functions are respectively defined by

$$\mathcal{H}(\phi(x)) = \begin{cases} 1, & \text{if } \phi(x) > 0, \\ 0, & \text{otherwise,} \end{cases} \quad (3.2)$$

and

$$\delta(\phi(x)) = \mathcal{H}'(\phi(x)). \quad (3.3)$$

According to [25], for any $f_2 = f_2(x)$, the following relation holds:

$$\int_{\partial\Omega} f_2 ds = \int_D \delta(\phi) |\nabla\phi| f_2 dx.$$

In the equation of state (2.1), the adjoint equation (2.8) and the Eulerian derivative (2.10), we use the Heaviside function for

$$k = k(\phi) = k_2(1 - \mathcal{H}(\phi)) + k_1\mathcal{H}(\phi).$$

The evolution of Ω and $\partial\Omega$ can be transformed into a transport equation of a time-dependent level set function $\phi = \phi(t, x)$ as

$$\begin{aligned}\frac{\partial\phi}{\partial t} + \mathcal{V} \cdot \nabla\phi &= 0 & \text{in } (0, \infty) \times D, \\ \phi(0, x) &= \phi_0(x) & \text{in } D, \\ \frac{\partial\phi}{\partial n} &= 0 & \text{on } (0, \infty) \times \partial D,\end{aligned} \quad (3.4)$$

where $\mathcal{V} : D \rightarrow \mathbb{R}^d$ is the velocity field and ϕ_0 is the initial level set function. During the optimization process, the level-set function usually becomes too flat, which causes numerical instability. One good way to overcome this problem is the level set function as a sign distance function

$$\phi(x) = \begin{cases} -\varphi(x; \Gamma) & \text{in } \Omega, \\ 0 & \text{on } \Gamma, \\ \varphi(x; \Gamma) & \text{in } D \setminus \Omega, \end{cases}$$

where

$$\varphi(x; \Gamma) := \min_{y \in \Gamma} \|x - y\|$$

denotes the minimal distance of x to Γ . For regularization of the level-set function, a so-called reinitialization process is usually suggested to be performed to the current level set function $\phi^0(x)$ by solving the solution $\psi = \psi(\tau, x)$ of the following nonlinear equation, up to the stationary state

$$\begin{aligned} \frac{\partial \psi}{\partial \tau} + \text{sign}(\phi)(|\nabla \psi| - 1) &= 0 && \text{in } (0, T) \times D, \\ \psi(0, x) &= \phi^0(x) && \text{in } D, \\ \frac{\partial \psi}{\partial n} &= 0 && \text{on } (0, T) \times \partial D, \end{aligned} \quad (3.5)$$

where sign is the sign function and $\tau > 0$ is a pseudo-time variable.

A H^1 -shape gradient flow is used to increase smoothness of velocity field [37]. More specifically, find $\mathcal{V} \in [H_0^1(D)]^d$ such that

$$\int_D (\omega \nabla \mathcal{V} : \nabla \mathcal{W} + \mathcal{V} \cdot \mathcal{W}) dx = -dJ(\Omega, \mathcal{W}) \quad \text{for all } \mathcal{W} \in [H_0^1(D)]^d, \quad (3.6)$$

where $\omega > 0$ is a parameter adjusting the diffusion effect. The gradient flow system involves the (vectorial) d -dimensional field whose numerical computations are demanding, especially in three-dimension. To reduce computational costs, we introduce a decomposition scheme which decomposes the d -dimensional problem (3.6) into d one-dimensional problems. More specifically, we can solve in parallel the scalar types of variational problems: Find $\mathcal{V}_i \in H_0^1(D)$ such that

$$\int_{\Omega} (\omega \nabla \mathcal{V}_i \cdot \nabla \eta + \mathcal{V}_i \eta) dx = -dJ(\Omega; \xi_i) \quad \text{for all } \eta \in H_0^1(D) \quad (3.7)$$

for $i = 1, 2, \dots, d$, where $\xi_i = [0, \dots, \eta, \dots, 0]^T$ with all components being 0 except the i -th being η . Set $\mathcal{V} = [\mathcal{V}_1, \mathcal{V}_2, \dots, \mathcal{V}_d]^T$. For efficient computing (3.7) with the finite element method, we assemble (stiffness and mass) matrices, perform LU decomposition only once and save them.

We use the characteristic finite element method [29, 40] to solve the level-set transport equation (3.4) [37, 40]. Let $X : \mathbb{R} \rightarrow \mathbb{R}^d$ such that

$$\frac{dX}{dt}(t) = \mathcal{V}(t, X(t)).$$

Then for $\phi : \mathbb{R} \times \mathbb{R}^d \rightarrow \mathbb{R}$, we have

$$\frac{d}{dt} \phi(t, X(t)) = \frac{\partial \phi}{\partial t} + \nabla \phi \cdot \mathcal{V},$$

where $\mathcal{V} = \mathcal{V}(t, \cdot)$ is the solution of (3.6) at each time t . This allows interpreting (3.4) as $(d/dt)\phi(t, X(t)) = 0$.

Let $\Delta t > 0$ be an appropriate time step. The backward Euler approximation of it is

$$\frac{d\phi}{dt}(t, X(t)) = \frac{\phi(t, X(t)) - \phi(t - \Delta t, X(t) - \mathcal{V}(t, X(t))\Delta t)}{\Delta t} + \mathcal{O}(\Delta t).$$

We consider the time discretization $0 = t_0 < t_1 < \dots < t_j$ with $t_j = j\Delta t (j \in \mathbb{N} \cup 0)$. The approximate solution at t_{j-1} by the Euler method is given by

$$X(t_{j-1}) = X(t_j) - \mathcal{V}(t_j, X(t_j))\Delta t + \mathcal{O}(\Delta t^2).$$

The above arguments imply that a first-order approximation of the material derivative is

$$\frac{d\phi}{dt}(t_j, X(t_j)) = \frac{\phi(t_j, X(t_j)) - \phi(t_{j-1}, X(t_{j-1}))}{\Delta t} + \mathcal{O}(\Delta t).$$

For $j = 1, 2, \dots$, the time semi-discretization of (3.4) reads: Find $\phi(t_j, X(t_j)) \in H^1(D)$ such that

$$\left(\frac{\phi(t_j, X(t_j)) - \phi(t_{j-1}, X(t_{j-1}))}{\Delta t}, v \right) = 0 \quad \text{for all } v \in H^1(D).$$

We also use the characteristics Galerkin method for reinitialization (3.5). We write it as

$$\psi_\tau + \mathcal{V} \cdot \nabla \psi = \text{sign}(\phi), \quad \mathcal{V} := \text{sign}(\phi) \frac{\nabla \psi}{|\nabla \psi|}.$$

For $l = 1, 2, \dots$, we use

$$\mathcal{V}(\tau_l, X(\tau_l)) := \text{sign}(\phi) \nabla \psi(\tau_l, X(\tau_l)) / |\nabla \psi(\tau_l, X(\tau_l))|.$$

The time semi-discrete variational form of (3.5) reads: Find $\psi(\tau_l, X(\tau_l)) \in H^1(D)$ such that

$$\left(\frac{\psi(\tau_l, X(\tau_l)) - \psi(\tau_{l-1}, X(\tau_{l-1}))}{\Delta \tau}, v \right) = (\text{sign}(\phi), v) \quad \text{for all } v \in H^1(D),$$

where

$$X(\tau_{l-1}) := X(\tau_l) - \mathcal{V}(\tau_l, X(\tau_l))\Delta \tau.$$

The sizes of Δt and $\Delta \tau$ are typically restricted for accuracy consideration and gradient descent requirement of the whole algorithm. We choose time step small enough for numerical accuracy, stability, and decrease of the objective [8]

$$\Delta t = c \frac{h}{\|V\|_{L^\infty(D)}},$$

where $c > 0$ is a suitable small parameter. Similar strategy is adopted for $\Delta \tau$.

Algorithm 2: A Level Set Method for Shape Reconstruction of Diffusive Interface

```

1 Initialization.
2 while Objective functional changes as iteration do
3   | Solve the state problem with Newton's method.
4   | Solve the adjoint state.
5   | Solve the shape gradient flow.
6   | Evolve the level-set equation.
7   if level set function becomes too flat or steep then
8     | Reinitialization.
9   else
10    | Go back.
11  end
12 end

```

Remark 3.1. Both algorithms described above can be stopped by a suitable criterion — viz. if the relative decrease of two successive objectives are smaller than a given error tolerance. Considering that inverse problems which can be very ill-posed in certain cases — e.g. highly noisy and/or in-sufficient observing data, we simply stop the algorithm.

Remark 3.2. Let us discuss advantages and disadvantages of Algorithms 1 and 2. Algorithm 1 is flexible for deformations through mesh moving and can be effective for shape optimization problems with topology of the subdomain to be reconstructed not known a priori. Secondly, it performs shape variations efficiently, especially for simple shapes and is relatively easy to implement. Algorithm 1 fails to deal with topological changes. Algorithm 2 is effective for complex shape optimization with no shape or topology information known a priori, since both shape and topological changes can happen by virtue of the level set method. Compared with Algorithm 1, Algorithm 2 although being mesh-fixed usually requires more computational efforts for solving level-set equation and reinitialization.

Remark 3.3. These algorithms should also be effective for a general nonlinear reaction term in (2.1) as long as the general reaction term ensures well-posedness of the state equation. Generally speaking, it is necessary to add growth restriction conditions to the nonlinear term [36]. More precisely, there is a positive constant C such that for all u , the following estimate holds:

$$|F(u)| \leq C(1 + |u|^{p-1}),$$

where $p = 6$ if $d = 3$, or $p \in [1, \infty)$ if $d = 2$. Moreover, the nonlinear term should satisfy Lipschitz continuity condition: there is a positive constant L such that

$$\|F(u_1) - F(u_2)\|_{H_0^1(D)} \leq L\|u_1 - u_2\|_{H_0^1(D)} \quad \text{for all } u_1, u_2 \in H_0^1(D).$$

4. Numerical Experiments

We test numerical performance of both algorithms. Set $k_1 = 1$ and $k_2 = 5$. The influence of added noise to observation data is considered in our numerical experiments. More specifically, we add noise to the exact finite element grid function u_d^* and then let u_d be the given data — i.e.

$$u_d = u_d^* + \sigma \frac{\|u_d^*\|_{L^2(D)}}{\|r^*\|_{L^2(D)}} r^*.$$

Here, $\sigma > 0$ is the noise level and r^* a grid function, whose nodal values are a uniform random distribution in $[-1,1]$ with zero mean value.

Notice that the Heaviside function (3.2) and delta function (3.3) are not differentiable. Thus they are numerically approximated respectively by

$$\mathcal{H}_\zeta(\phi) = \begin{cases} 0, & \text{if } \phi < -\zeta, \\ \frac{1}{2} + \frac{\phi}{2\zeta} + \frac{1}{2\pi} \sin\left(\frac{\pi\phi}{\zeta}\right), & \text{if } |\phi| \leq \zeta, \\ 1, & \text{if } \phi > \zeta, \end{cases}$$

$$\delta_\zeta(\phi) = \begin{cases} 0, & \text{if } |\phi| > \zeta, \\ \frac{1}{2\zeta} + \frac{1}{2\zeta} \cos\left(\frac{\pi\phi}{\zeta}\right), & \text{if } |\phi| \leq \zeta \end{cases}$$

with a small parameter $\zeta > 0$. We use the approximation [25, 28] for numerically computing $\text{sign}(\phi)$

$$\text{sign}(\phi) \simeq \frac{\phi}{\sqrt{\phi^2 + h^2|\nabla\phi|^2}}.$$

4.1. Examples of Algorithm 1

Example 4.1. Choose a square $D = (-1, 1)^2$. The target subdomain Ω is a disk $\{x|x_1^2 + x_2^2 \leq 0.5\}$. We test two cases for the initial Ω : a square located in the center and a non-convex L-shape. Let $M = D$ and $\sigma = 0$ for the first two cases. For Case 1, Fig. 2 shows that the use of conformal mapping ($\gamma = 10^{-3}$) allows good shape-regular mesh qualities during mesh moving and set regularization parameter $\alpha = 10^{-4}$. The reconstruction effect is satisfactory. See Fig. 3 for Case 2 ($\alpha = 10^{-5}$), instead of using conformal mapping, remeshing is employed every 5 iterations. In this way, good mesh quality can be maintained at the expense of additional computational effort. The convergence history of the objective for both cases is shown in Fig. 4. Finally, we test partial measurement and noisy observation in Case 3. Choose

$$M = (-1, 1)^2 \setminus [-0.8, 0.8]^2$$

and $\sigma = 0.01$. Set $\alpha = 10^{-8}$. Fig. 5 shows the reconstruction and Fig. 6 shows the convergence history. The comparisons on the reconstruction result and the final objective between the noise free and noisy cases indicate better reconstruction effect for the noisy free case, which is a expected phenomenon.

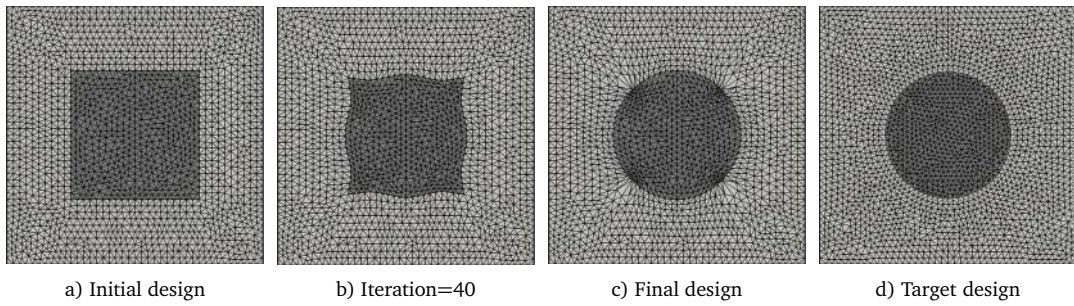


Figure 2: Example 4.1, Case 1. Shape changes with conformal mapping used.

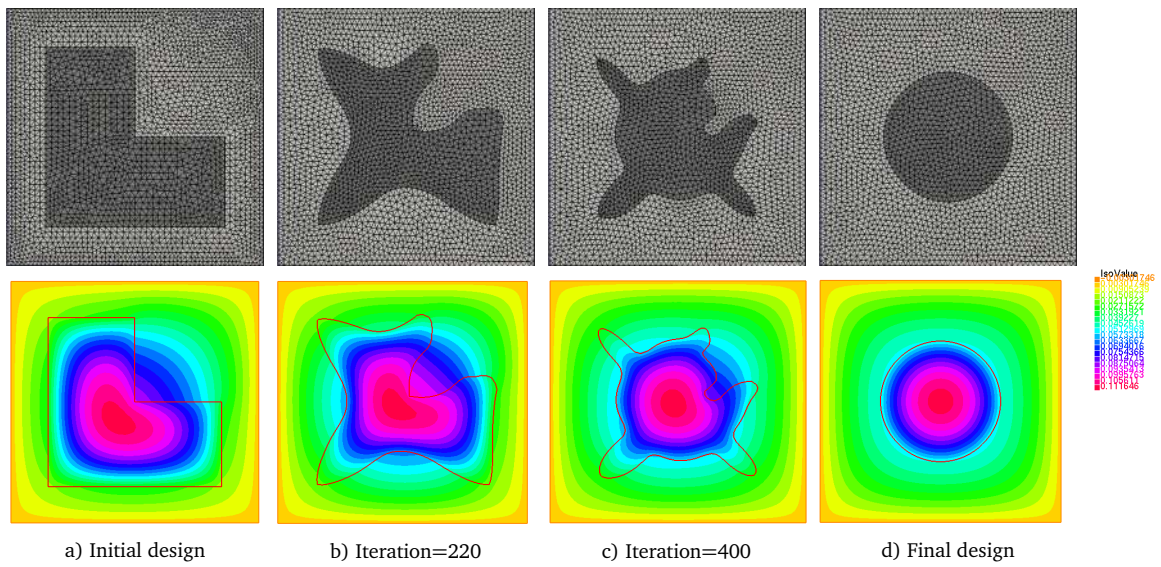


Figure 3: Example 4.1, Case 2. Shape deformations (first row) and corresponding finite element solutions (second row).

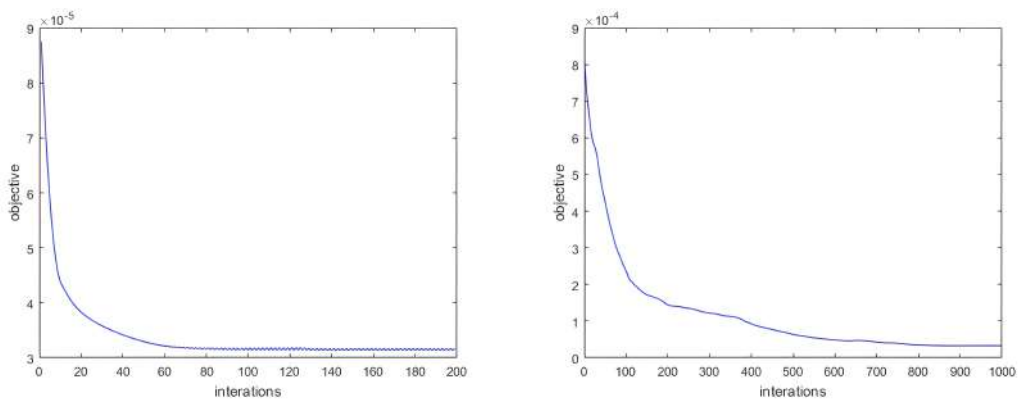


Figure 4: Example 4.1. Convergence history: Case 1 (left) and Case 2 (right).

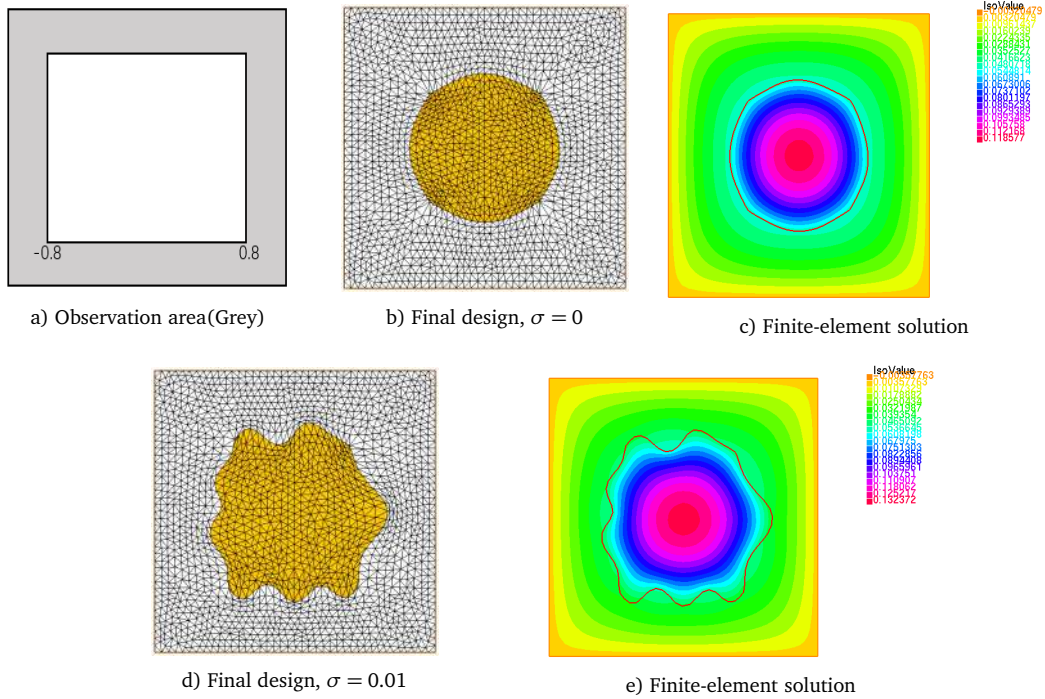


Figure 5: Example 4.1, Case 3. Reconstruction results.

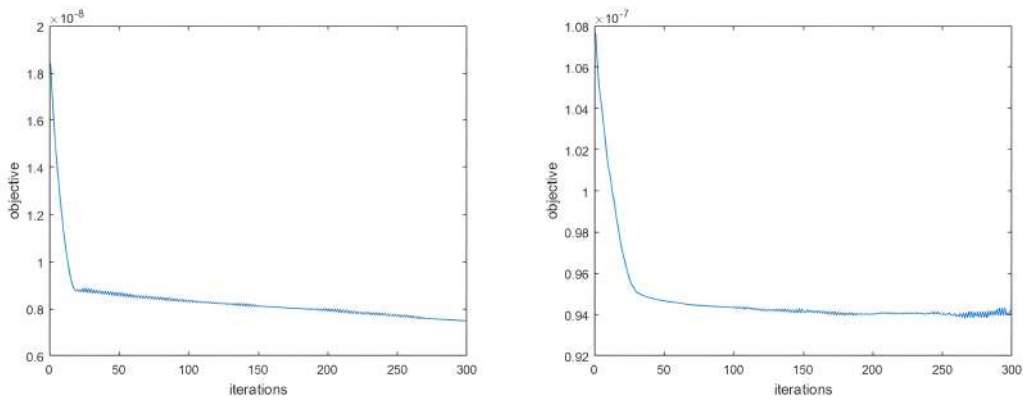


Figure 6: Example 4.1, Case 3. Convergence history: $\sigma = 0$ (left) and $\sigma = 0.01$ (right).

Example 4.2. Set $D = (0, 1)^2$. The target Ω is non-convex. We test two cases for the initial Ω : a square located in the center and an L-shape. Set $\alpha = 10^{-5}$. As shown in Fig. 7 with conformal mapping ($\gamma = 10^{-3}$) for Case 1, the shape evolution process illustrates the effectiveness of final reconstruction from initial square. Fig. 8 shows the unsatisfactory result without conformal mapping and the satisfactory result with remeshing. When conformal mapping is not used and the mesh is not redivided, in the process of optimization, because the mesh quality is too poor, the optimization step will continue to decrease or even tend

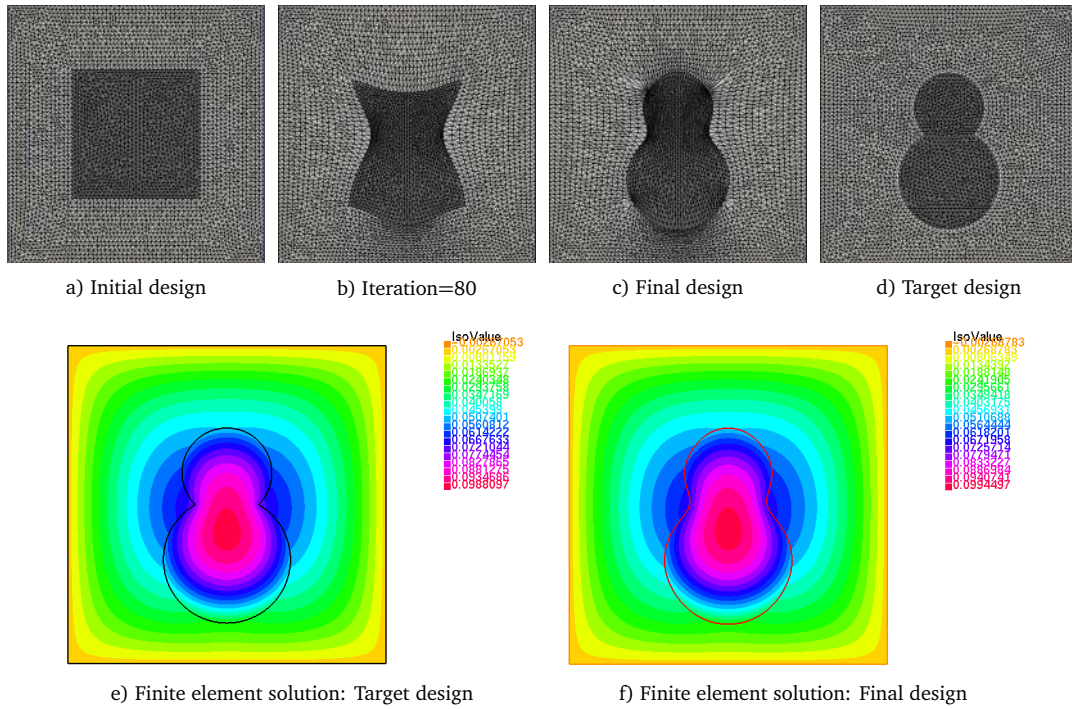


Figure 7: Example 4.2, Case 1. Reconstruction process.

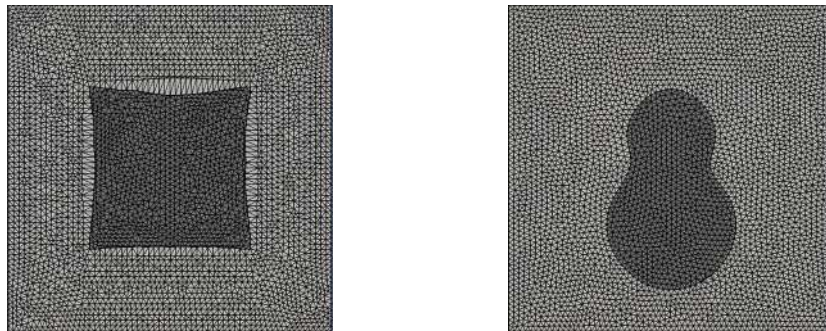


Figure 8: Example 4.2, Case 1. Reconstructed result without conformal mapping (left) and with remeshing (right).

to 0, so that the optimization cannot continue. In Fig. 9, convergence histories of the objective show the algorithm without using conformal mapping and remeshing leads to poor final result, while either remeshing or conformal mapping is effective for algorithm's convergence. In Case 2, Figs. 10 and 11 show the shape evolution process with remeshing used every 5 iterations and convergence history of the objective, respectively. We also consider the optimization with only partial measurement and noise $\sigma = 0.01$. The observation data is shown in Fig. 5(a), and the optimization result is shown in Fig. 10(h). Here, set $\alpha = 10^{-8}$, and other parameter values are not changed.

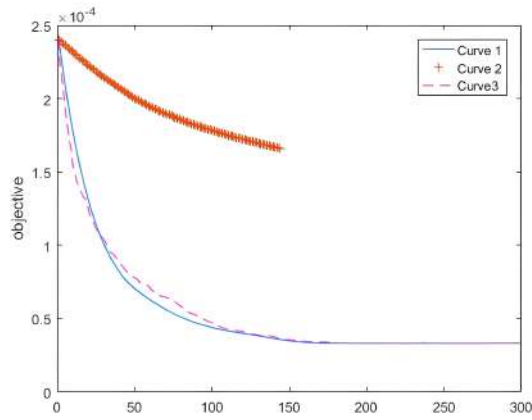


Figure 9: Example 4.2, Case 1. Convergence histories: without using conformal mapping (Curve 2), using conformal mapping (Curve 1), and using remeshing (Curve 3).

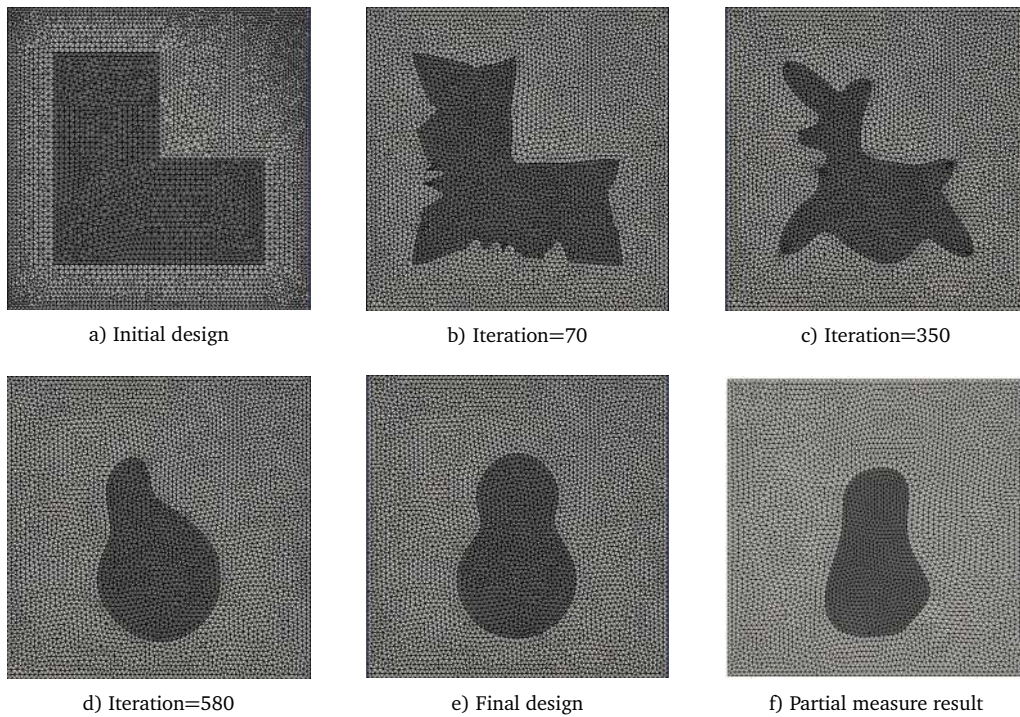


Figure 10: Example 4.2, Case 2. Shape evolution process.

Example 4.3. Consider reconstruction on an irregular D in Fig. 12 for satisfactory results obtained with $\alpha = 10^{-5}$. In this example, we also consider the optimization based on partial observation data shown in Fig. 12(a) and add noise, where the noise level $\sigma = 0.01$ and set $\alpha = 10^{-9}$. The optimization result is shown in Fig. 12(d).

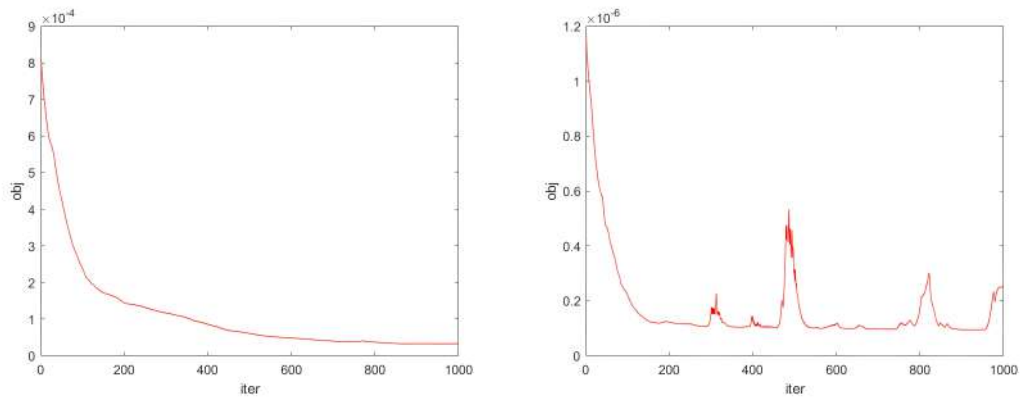


Figure 11: Example 4.2, Case 2. Convergence history: $\alpha = 10^{-5}$ (left) and $\alpha = 10^{-8}$ (right).

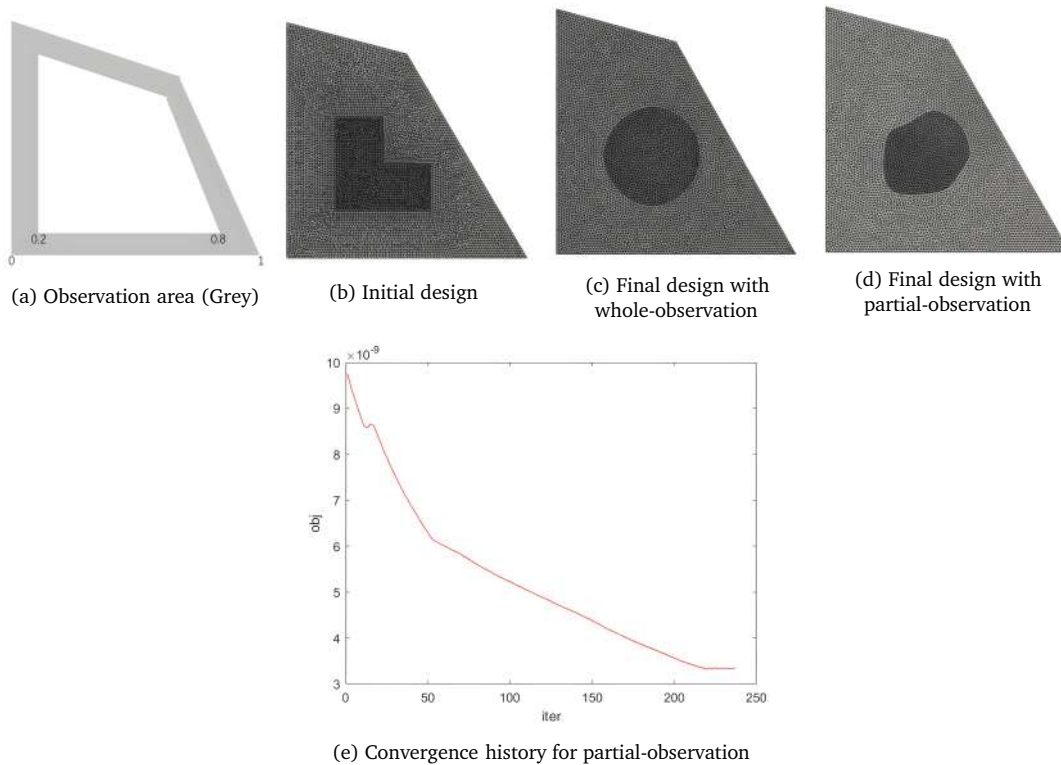


Figure 12: Example 4.3, Algorithm 1. Final design, $\sigma = 0$, $\alpha = 10^{-5}$ (c) and $\sigma = 0.01$, $\alpha = 10^{-9}$ (d).

4.2. Examples of Algorithm 2

Both shape and topology changes are allowed using the level set method with fixed meshes on general design regions as shown below. Set $\omega = 10^{-3}$, cf. (3.6). We reinitialize at every iteration.

Example 4.4. We solve Example 4.3 by the level set method, which allows shape changes on fixed irregular design region as shown in Fig. 13. The final reconstruction of noisy case ($\sigma = 0.01$) is slightly less satisfactory than the noise-free one as expected, especially when partial observation data is available as shown in Fig. 12(a). In Fig. 14, as α increases, there is more regularization effect and thus the interface length is expected to decrease.

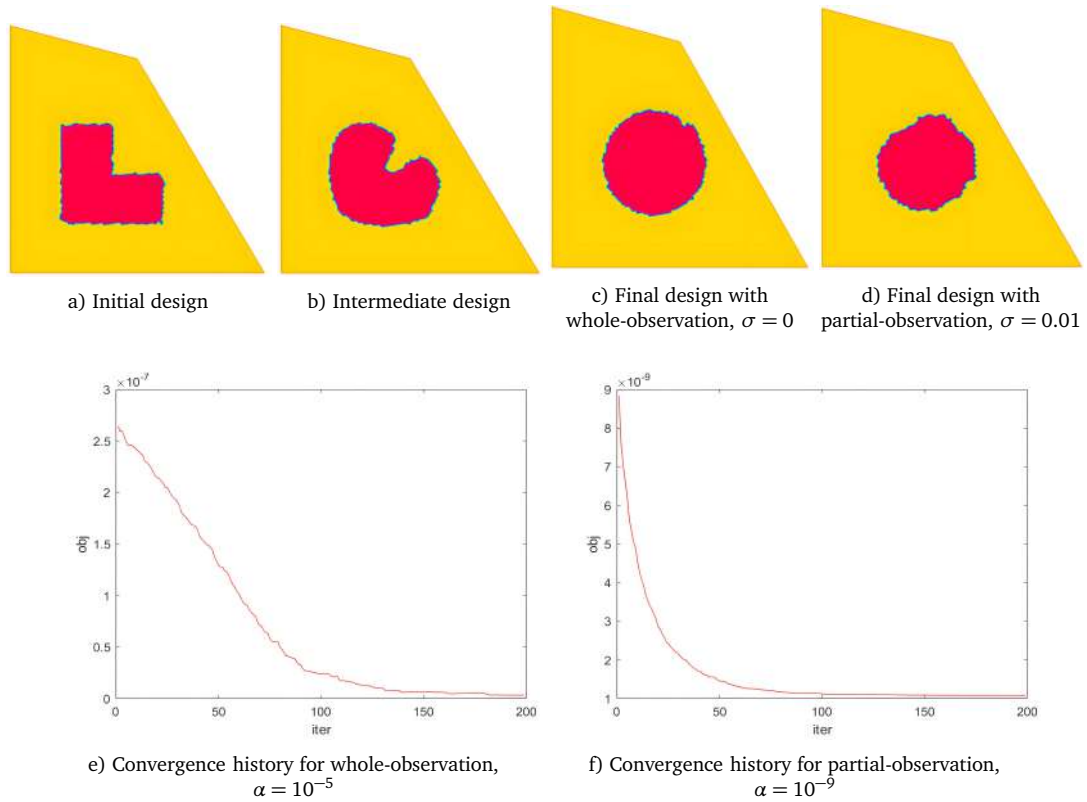


Figure 13: Example 4.4 by Algorithm 2. Optimization process and convergence history.

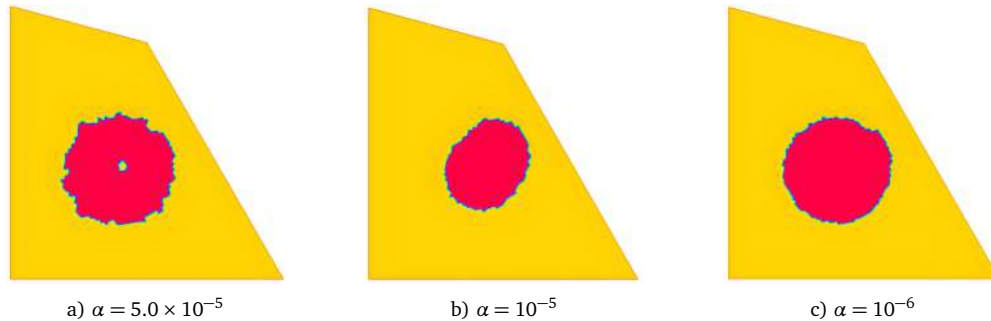


Figure 14: Example 4.4. Effects of the regularization parameter on reconstruction results, $\sigma = 0.1$.

Example 4.5. Choose $D = (0, 1)^2$, cf. Fig. 15. We reconstruct a diamond and an ellipse. Set $\alpha = 10^{-5}$. The evolution process is shown in Fig. 16, where satisfactory reconstruction results are obtained with noise-free whole-observation. Both initial designs with several holes and one hole can converge to a well multi-connected reconstruction result. Similar to Case 3 of Example 4.1, we consider the same partial observation as in Fig. 5(a).

In Fig. 17, as the observation data information reduces, the reconstruction quality decreases compared with the reconstruction result in Fig. 16. Moreover, the reconstruction quality decreases further when data has noise. From Fig. 18, the comparisons of the two cases show that the final objective value of the noisy case is reasonably larger.

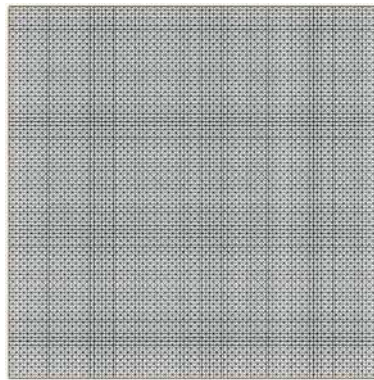


Figure 15: Examples 4.5-4.6. Mesh of $D = (0, 1)^2$.

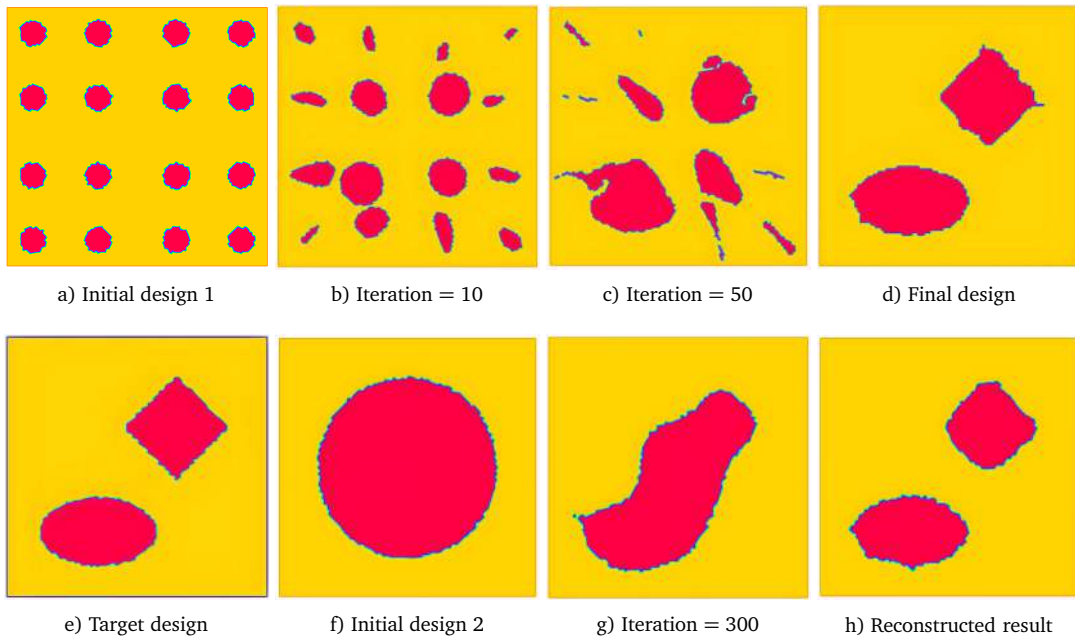


Figure 16: Example 4.5. Shape and topological changes with noise-free whole-observation.

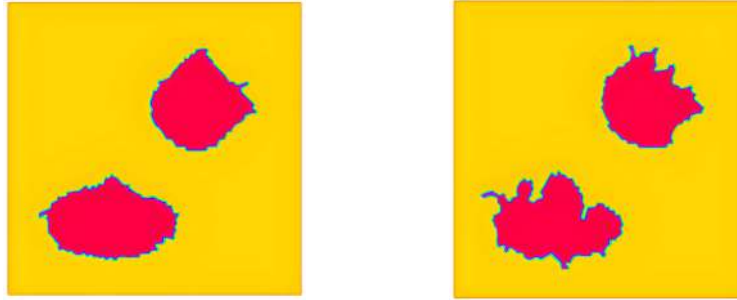


Figure 17: Example 4.5 with partial measurement, $\sigma = 0$ (left) and $\sigma = 0.01$ (right).

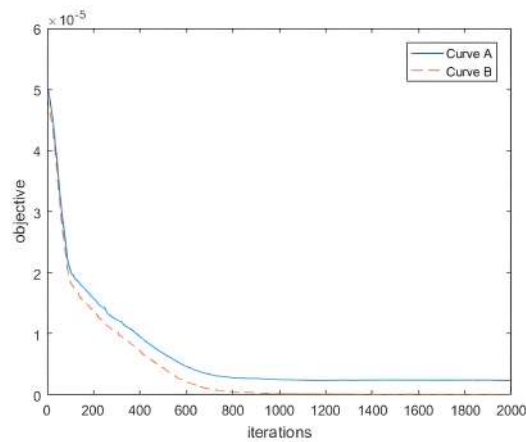


Figure 18: Example 4.5 with partial measurement: Convergence history (Curve A, $\sigma = 0.01$ and Curve B, $\sigma = 0$).

Example 4.6. We re-solve Example 4.2 with Algorithm 2. Choose $\alpha = 10^{-9}$. The algorithm allowing topological changes starts with an initial design containing a few holes as shown in Fig. 19, where the final concave object is approximately reconstructed. It is expected that the partial observation reconstruction with $\sigma = 0.01$ is not so good as the whole observation one. In Fig. 20, the partial observation case converges to a slightly higher value than the whole observation case for convergence history of the objective.

Example 4.7. Let $D = (0, 1)^3$. Choose the target Ω to be a heart-shaped region as shown in Fig. 21(f). Set $\alpha = 10^{-9}$. Fig. 21 shows the noisy case has lower reconstruction quality than the noise-free one. Both multi-connected and simply-connected initial subdomains can converge to the heart shape, which implies the robustness of Algorithm 2 in 3D. Moreover, the more practical case with only partial observation data and noise is also considered, in which $M := (-1, 1)^3 \setminus [-0.8, 0.8]^3$ and $\sigma = 0.01$. See Figs. 22 and 23 for reconstruction and convergence history of objective. Choose $\alpha = 10^{-8}$. As expected for whole-observation, the converged objective of the noisy data case is larger than that of the noise-free one in Fig. 23.

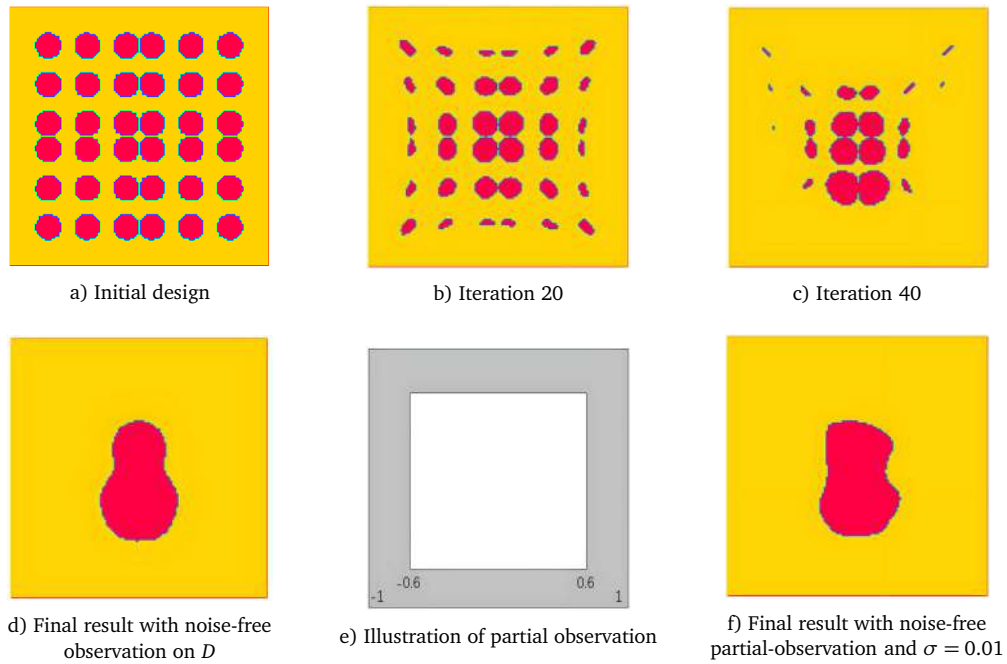
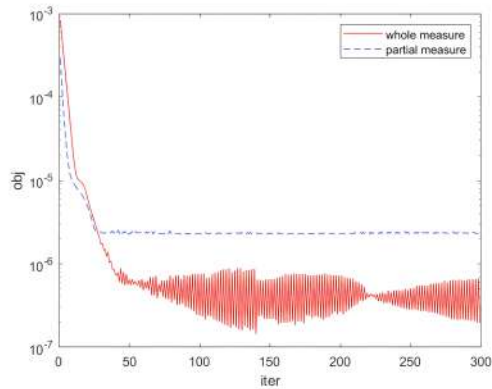


Figure 19: Example 4.6. Optimization process.

Figure 20: Example 4.6. Convergence history: $\alpha = 10^{-9}$.

5. Conclusion

We have shown existence and proposed numerical methods for solving an inverse shape problem associated with a semi-linear elliptic interface problem in reaction diffusion. We performed shape sensitivity analysis and used the distributed shape gradient to propose a numerical shape optimization algorithm and a topology optimization algorithm, the latter of which is based on the level set method. A variety of numerical examples were proposed to demonstrate the effectiveness of our algorithms.

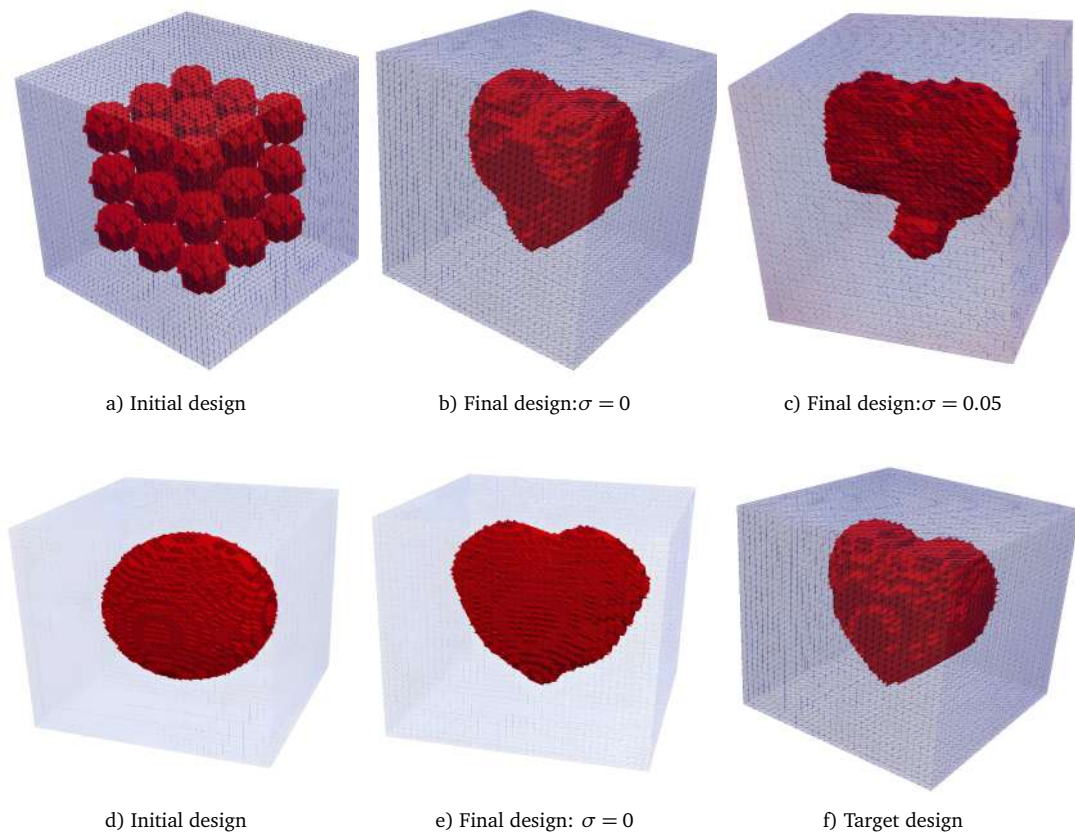


Figure 21: Example 4.7. Initial and reconstructed results.

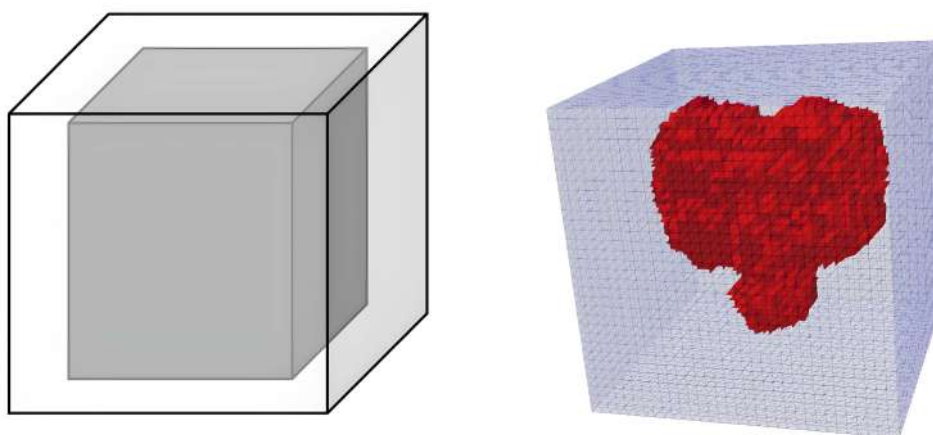


Figure 22: Example 4.7. Left: Partial observation illustration (White region). Right: Reconstruction result, $\sigma = 0.01$.

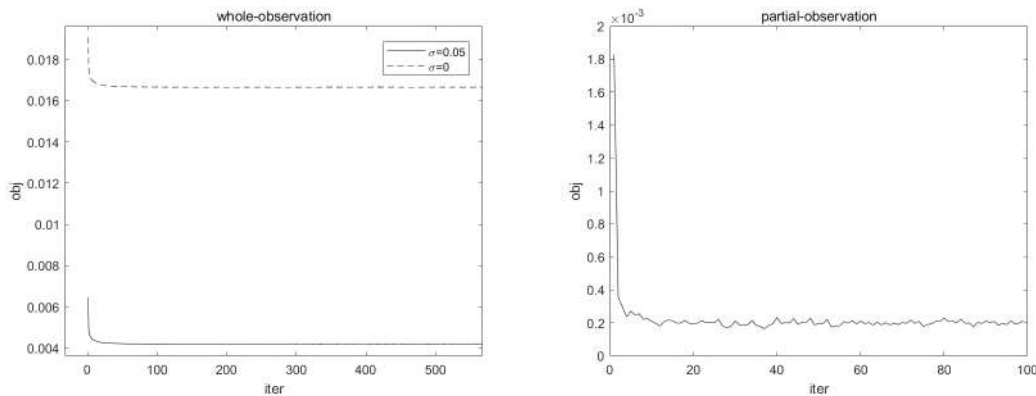


Figure 23: Example 4.7. Convergence history: Whole-observation (left) and partial-observation (right).

Acknowledgments

The authors thank the anonymous referees for their valuable comments.

This work was supported in part by the National Key Basic Research Program (Grant No. 2022YFA1004402), by the Science and Technology Commission of Shanghai Municipality (Grant Nos. 21JC1402500, 22ZR1421900, 22DZ2229014), and by the National Natural Science Foundation of China (Grant No. 12071149).

References

- [1] G. Allaire, C. Dapogny and F. Jouve, *Shape and topology optimization, in geometric partial differential equations. Part II*, Handbook of Numerical Analysis, Elsevier **22**, 1–132 (2021).
- [2] H.B. Ameur, M. Burger and B. Hackl, *Level set methods for geometric inverse problems in linear elasticity*, Inverse Prob. **20**, 673–696 (2004).
- [3] E. Beretta, A. Manzoni and L. Ratti, *A reconstruction algorithm based on topological gradient for an inverse problem related to a semilinear elliptic boundary value problem*, Inverse Prob. **33**, (2017).
- [4] E. Beretta, S. Micheletti, S. Perotto and M. Santacesaria, *Reconstruction of a piecewise constant conductivity on a polygonal partition via shape optimization in EIT*, J. Comput. Phys. **353**, 264–280 (2018).
- [5] E. Beretta, L. Ratti and M. Verani, *Detection of conductivity inclusions in a semilinear elliptic problem arising from cardiac electrophysiology*, Commun. Math. Sci. **16**, 1975–2002 (2018).
- [6] M. Berggren, *A unified discrete-continuous sensitivity analysis method for shape optimization*, in: Applied and Numerical Partial Differential Equations, Springer 25–39 (2010).
- [7] E. Burman, D. Elfverson, P. Hansbo, M.G. Larson and K. Larsson, *Shape optimization using the cut finite element method*, Comput. Methods Appl. Mech. Engrg. **328**, 242–261 (2018).
- [8] M. Burger, *A framework for the construction of level set method for shape optimization and reconstruction*, Interfaces and Free Bound. **5**, 301–329 (2003).
- [9] Y. Chen, Q. Li, Y. Wang and Y. Huang, *Two-grid methods of finite element solutions for semi-linear elliptic interface problems*, Numer. Algorithms. **84**, 307–330 (2020).
- [10] E.T. Chung, T.F. Chan and X.C. Tai, *Electrical impedance tomography using level set representa-*

- tion and total variational regularization, *J. Comput. Phys.* **205**, 357–372 (2005).
- [11] M.C. Delfour and J.P. Zolesio, *Shapes and Geometries. Metrics, Analysis, Differential Calculus and Optimization*, SIAM (2011).
- [12] P. Gangl, U. Langer, A. Laurain, H. Meftahi and K. Sturm, *Shape optimization of an electric motor subject to nonlinear magnetostatics*, *SIAM J. Sci. Comput.* **37**, B1002–B1025 (2015).
- [13] J. Haslinger and R.A.E. Mäkinen, *Introduction to Shape Optimization. Theory, Approximation and Computation*, SIAM (2003).
- [14] F. Hettlich and W. Rundell, *Iterative methods for the reconstruction of an inverse potential problem*, *Inverse Prob.* **12**, 251–266 (1996).
- [15] R. Hiptmair, A. Paganini and S. Sargheini, *Comparison of approximate shape gradients*, *BIT Numer. Math.* **55**, 459–485 (2015).
- [16] X. Hu and S. Zhu, *On geometric inverse problems in time-fractional subdiffusion*, *SIAM J. Sci. Comput.* **44**, A3560–A3591 (2022).
- [17] J.A. Iglesias, K. Sturm and F. Wechsung, *Two-dimensional shape optimization with nearly conformal transformations*, *SIAM J. Sci. Comput.* **40**, A3807–A3830 (2018).
- [18] M. Iguernane, S. Nazarov, J.-R. Roche, J. Sokolowski and K. Szulc, *Topological derivatives for semilinear elliptic equations*, *Int. J. Appl. Math. Comput. Sci.* **19**, 191–205 (2009).
- [19] K. Ito, K. Kunisch and Z. Li, *Level-set function approach to an inverse interface problem*, *Inverse Probl.* **17**, 1225–1242 (2001).
- [20] B. Jin, Y. Xu and J. Zou, *A convergent adaptive finite element method for electrical impedance tomography*, *IMA J. Numer. Anal.* **37**, 1520–1550 (2017).
- [21] B. Jin and Z. Zhou, *Error analysis of finite element approximations of diffusion coefficient identification for elliptic and parabolic problems*, *SIAM J. Numer. Anal.* **59**, 119–142 (2021).
- [22] A. Laurain and K. Sturm, *Distributed shape derivative via averaged adjoint method and applications*, *ESAIM Math. Model. Numer. Anal.* **50**, 1241–1267 (2016).
- [23] J. Li and S. Zhu, *Shape optimization of Navier-Stokes flows by a two-grid method*, *Comput. Methods Appl. Mech. Engrg.* **400**, (2022).
- [24] C. Liu and S. Zhu, *A semi-implicit binary level set method for source reconstruction problems*, *Int. J. Numer. Anal. Model.* **8**, 410–426 (2011).
- [25] S. Osher and R. Fedkiw, *Level Set Methods and Dynamic Implicit Surfaces*, Springer (2003).
- [26] S. Osher and J.A. Sethian, *Front propagation with curvature dependent speed: Algorithms based on Hamilton-Jacobi formulations*, *J. Comput. Phys.* **79**, 12–49 (1988).
- [27] C.V. Pao, *Nonlinear Parabolic and Elliptic Equations*, Plenum (1992).
- [28] D. Peng, B. Merriman, S. Osher, H. Zhao and M. Kang, *A PDE-based fast local level set method*, *J. Comput. Phys.* **155**, 410–438 (1999).
- [29] O. Pironneau, *On the transport-diffusion algorithm and its applications to the Navier-Stokes equations*, *Numer. Math.* **38**, 309–312 (1982).
- [30] F. Santosa, *A level-set approach for inverse problems involving obstacles*, *ESAIM Control Optim. Calc. Var.* **1**, 17–33 (1995).
- [31] J.F. Scheid, J. Sokolowski and K. Szulc, *A numerical method for shape and topology optimization for semilinear elliptic equation*, 15th International Conference on Methods and Models in Automation and Robotics, (2010).
- [32] V. Schulz, M. Siebenborn and K. Welker, *Structured inverse modeling in parabolic diffusion problems*, *SIAM J. Contr. Optim.* **53**, 3319–3338 (2015).
- [33] J. Sokolowski and J.P. Zolesio, *Introduction to Shape Optimization: Shape Sensitivity Analysis*, Springer (1992).
- [34] K. Sturm, *Topological sensitivities via a Lagrangian approach for semilinear problems*, *Nonlinearity* **33**, 4310–4337 (2020).

- [35] K. Sturm, M. Hintermüller and D. Hömberg, *Distortion compensation as a shape optimisation problem for a sharp interface model*, *Comput. Optim. Appl.* **64**, 557–588 (2016).
- [36] M. Wang, *Nonlinear Elliptic Equations (in Chinese)*, Science Press (2010).
- [37] K. Yaji, M. Otomori, T. Yamada, K. Izui, S. Nishiwaki and O. Pironneau, *Shape and topology optimization based on the convected level set method*, *Struct. Multidiscip. Optim.* **54**, 659–672 (2016).
- [38] S. Zhu, *Effective shape optimization of Laplace eigenvalue problems using domain expressions of Eulerian derivatives*, *J. Optim. Theory and Appl.* **176**, 17–34 (2018).
- [39] S. Zhu and Z. Gao, *Convergence analysis of mixed finite element approximations to shape gradients in the Stokes equation*, *Comput. Methods Appl. Mech. Engrg.* **343**, 127–150 (2019).
- [40] S. Zhu, X. Hu and Q. Wu, *A level set method for shape optimization in semilinear elliptic problems*, *J. Comput. Phys.* **355**, 104–120 (2018).